

# A Sawtooth Permanent Magnetic Lattice for Ultracold Atoms and BECs

Amir Mohamadi and Saeed Ghanbari

Department of Physics, Faculty of Science, University of Zanjan, P.O. Box 45195-313, Zanjan, Iran

Received: date / Revised version: date

**Abstract.** We propose a new permanent magnetic lattice for creating periodic arrays of Ioffe-Pritchard permanent magnetic microtraps for holding and controlling ultracold atoms and Bose-Einstein condensates (BECs). Lattice can be designed on thin layer of magnetic films such as  $Tb_6Gd_10Fe_{80}Co_4$ . In details, we investigate single layer and two crossed layers of sawtooth magnetic patterns with thicknesses of 50 and 500nm respectively with a periodicity of  $1\mu\text{m}$ . Trap depth and frequencies can be changed via an applied bias field to handle tunneling rates between lattice sites. We present analytical expressions and using numerical calculations show that this lattice has non-zero potential minima to avoid majorana spin flips. One advantage of this lattice over previous ones is that it is easier to manufacture.

**PACS.** 67.85.Hj ,67.85.Jk,37.10.Gh,37.10.De,85.85.+j

## 1 Introduction

Focused laser beams have been used extensively in years for cooling atoms and molecules to hold them [1,2,3,4,5]. These optical traps are made by a radiation field whose intensity has a maximum in space. Due to interaction with electric field of laser, small clouds of atoms can be confined, manipulated and controlled in optical lattices [6,7,8]. Radiation absorption and induced dipole forces constrain atoms to optical lattice [9]. Periodic optical lattices are the result of interference of intersecting laser beams and have allowed for the observation of the Mott-insulator to superfluid transition [10,11], studies of low-dimensional and quantum degenerate gases [12,13] and coherent molecules [14]. In quantum computation, optical lattices provide a large qubit system and produce gate operations on the register [15,16].

Using magnetic field is another approach to realize harmonic potential in space [17]. Magnetic lattices are created using periodically magnetized films or current carrying wires on atom chips [18,19,20,21,22]. These magnetic potentials are promising alternatives to the optical lattices and provide a high degree of design flexibility, arbitrary geometries and lattice spacing. Magnetic lattices can produce highly stable periodic potential wells with low noise [23]. Single 3D magnetic microtraps also have been introduced either by current carrying wires or permanent magnetic slabs [24,25]. Recently, development of technology has let us for working on high-quality magnetic materials based on permanent, perpendicularly magnetized films [26,27]. Periodic grooved magnetic mirrors

have been made by the technology of thin films to reflect ultracold atoms [28]. In the presence of magnetic bias fields, mirrors are transferred into 1D arrays of 2D waveguides and 2D arrays of 3D traps [18]. Magnetic films such as  $Tb_6Gd_10Fe_{80}Co_4$  have excellent magnetic properties; homogeneity, high magnetization, large coercivity ( $H_c \sim 3\text{kO}_e$ ) and high Curie temperature( $\sim 300^\circ\text{C}$ ) [18,19].

In this paper, we introduce a new atom chip based on permanent periodic grooved magnetic film and external magnetic fields. This sawtooth magnetic lattice is proposed for controlling, manipulating and trapping clouds of ultracold atoms when they are in low-field seeking states. Analytical expressions and numerical calculations show that the magnetic field minima are non-zero. Therefore, ultracold atoms can be hold and trapped without any spin flips in lattice sites. In particular, we investigate 1D array of this grooved magnetic lattice, when bias fields are applied. Results show that produced waveguides have controllable depth and frequencies to handle clouds of quantum degenerate gases on the chip surface. We show that two crossed separated layers of periodic arrays also can produce 2D magnetic lattice of 3D microtraps when bias fields are applied. The microtraps have non-zero minimum and high depth ( $\sim 0.2\text{mK}$ ) which cause prevention of majorana spin flips and efficient restriction of trapped atoms, respectively. Magnetic atom chips based on permanent magnetic materials have some advantages over optical or microwire devices. Since there is no spontaneous emission due to decay of excited atoms, light scattering and decoherence of cold atoms vanishes and no beam alignment is required [9]. Heat dissipation and loss of atoms due to fluctuation of current in current-carrying microwires

Correspondence to: amir.m@znu.ac.ir, sghanbari@znu.ac.ir

are prevented in permanent magnetic lattices. They can produce large field curvatures, large trap depth and high frequencies with very low technical noises [23]. The main motivation of this work is introducing a more flexible permanent magnetic lattice compared with the configuration of the two crossed arrays of rectangular permanent magnetic slabs proposed in [18]. Considering the shape of this new atom chip, current technology in grooving of films for magnetic mirrors allows us to produce it more easily compared with previous ones.

## 2 Analytical expressions for Magnetic lattices

We study first the simple case of a single layer of sawtooth periodic array of grooved magnetic films with a thickness of  $t$ , periodicity  $a$  along the  $y$ -direction, magnetization  $M = M_z \hat{z}$  and constant bias magnetic fields  $B_{1x}$ ,  $B_{1y}$  and  $B_{1z}$  along the  $x$ -,  $y$ - and  $z$ -directions.

### 2.1 Atom waveguide

The configuration of the permanent magnets is shown in Fig.1. Pattern of magnetic film has a periodicity (distance between two alternative peaks) of  $a = 1\mu\text{m}$  and a thickness of  $t = 500\text{nm}$  while dimensions of lattice in  $x$ - and  $y$ -directions,  $l_x$  and  $l_y$  are  $1\text{mm}$  (Fig.1(c)). For analytical and numerical calculations, we approximate our sawtooth magnetic pattern thin rectangular magnetic slabs same magnetization and periodicity but with different widths. As Fig.1 (a) shows, infinite periodic arrays of magnets are placed above each other to shape sawtooth structure. At a large distance where  $k(z - t) \gg 1$ , the using expressions given in Ref. [18], the components of the magnetic field can be written

$$B_x = B_{1x} \quad (1)$$

$$B_y = B_{0\gamma} \sin(ky) e^{-kz} + B_{1y}$$

$$B_z = B_{0\gamma} \cos(ky) e^{-kz} + B_{1z}$$

where  $k = 2\pi/a$  and  $B_{0\gamma} = B_0 \sum_{i=0}^{n-1} \gamma_i$ , respectively.  $B_0$  and  $\gamma_i$  are  $M_z/\pi$  (Gaussian units) and related coefficient of the  $i$ th infinite periodic magnets on atom chip [see Fig.1(b)], respectively.  $\gamma_i$  is determined from the series [for more details, see section 2.3]

$$\gamma_i = \frac{1}{A} \sum_{j=0}^i \cos\left(\frac{(2j+1)ka}{4n}\right) (e^{k\frac{j}{n}} - 1) e^{kt(1-\frac{(i+1)}{n})} \quad (2)$$

$$A = \sum_{j=0}^{n/2-1} \cos\left(\frac{(2j+1)ka}{4n}\right)$$

where  $n$  is the number of sub-layers (i.e. order of approximation). The magnitude of the magnetic field above surface can be written

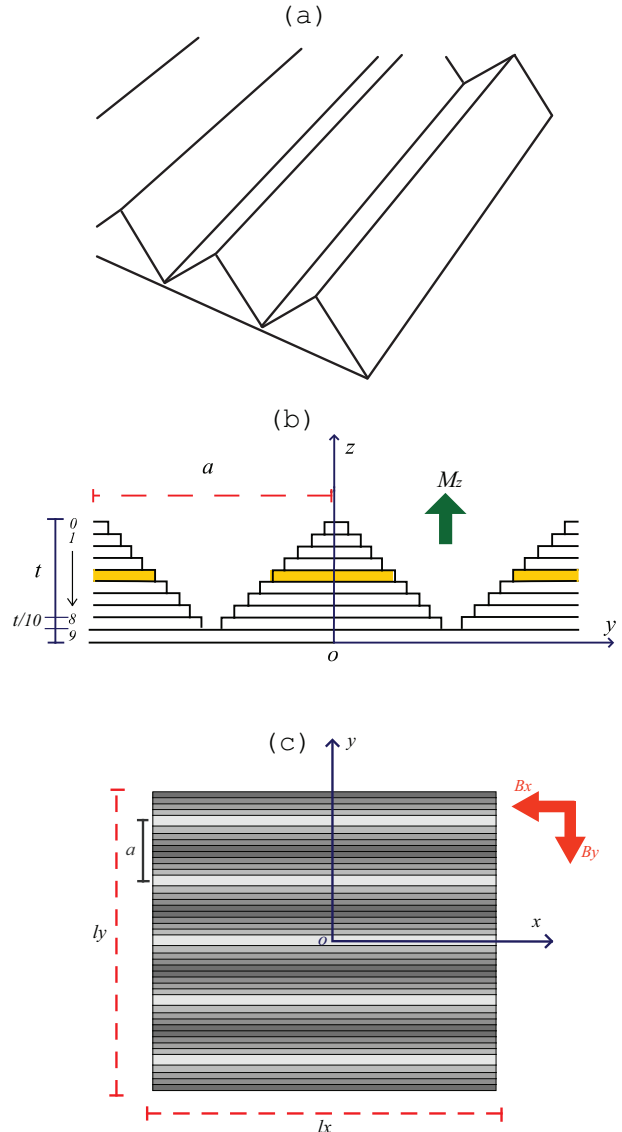


**Fig. 1.** (Color online) (a) 1D array of sawtooth permanent magnetic lattice. (b) Schematic of sawtooth permanent magnetic lattice film which has been estimated by  $n=10$  sub-layers of rectangular magnetic slabs. Periodicity of the sawtooth permanent magnetic lattice is the periodicity of the rectangular slabs and is defined by distance of two alternative peaks of the structure. Lattice has the periodicity  $a=1\mu\text{m}$ , magnetization  $M_z=3.8\text{ kG}$  along the  $z$ -direction and thickness  $t=500\text{nm}$ . For  $n=10$ , thickness of each sublayer is  $t/n=50\text{nm}$  while width of slabs is changed according to  $w_i=a(i+1)/n$ . (c)  $l_x$  and  $l_y$ , dimensions of the atom chip in  $x$ - and  $y$ -directions, respectively. For  $n_r=1000$  sawtooth magnetic slabs  $l_x=l_y=1\text{mm}$ . External magnetic field is applied along  $x$ - and  $y$ -directions to produce waveguides with non-zero potential minima.

$$B(y, z) = (B_{1x}^2 + B_{1y}^2 + B_{1z}^2 + 2[B_{0\gamma}B_{1y} \sin(ky) + B_{0\gamma}B_{1z} \cos(ky)]e^{-kz} + B_{0\gamma}^2e^{-2kz})^{1/2} \quad (3)$$

In simple case when we take  $B_{1z}=0$ , the minimum of magnetic field in 1D array of periodic magnetic lattice of 2D microtraps is

$$B_{\min} = |B_{1x}| \quad (4)$$

where the center of the waveguides are located at

$$y_{\min} = (n_y + \frac{1}{4})a \quad (5)$$

$$z_{\min} = \frac{1}{k} \ln \left( \frac{B_{0\gamma}}{|B_{1y}|} \right)$$

where  $n_y$  is the trap number in the  $y$ -direction and takes values of  $0, \pm 1, \pm 2, \dots$ .

According to equation 4, the  $x$  component of the bias field is necessary to avoid spin flips near the center of 2D microtraps. The magnetic barrier heights along  $y$ - and  $z$ -directions which depend on the bias fields are given by

$$\Delta B^y = B_{\max}^y - B_{\min} = (B_{1x}^2 + 4B_{1y}^2)^{1/2} - |B_{1x}| \quad (6)$$

$$\Delta B^z = B_{\max}^z - B_{\min} = (B_{1x}^2 + B_{1y}^2)^{1/2} - |B_{1x}|$$

Second derivatives (curvatures) of the magnetic field at the minimum of the potential and trap frequencies of the waveguides along  $y$ - and  $z$ -directions could be analytically determined by

$$\frac{\partial^2 B}{\partial y^2} = \frac{\partial^2 B}{\partial z^2} = k^2 \frac{B_{1y}^2}{|B_{1x}|} \quad (7)$$

$$\omega_y = \omega_z = kB_{1y} \left( \frac{\mu_B g_F m_F}{m B_{1x}} \right)^{1/2} \quad (8)$$

where  $\mu_B$ ,  $g_F$ ,  $m_F$  and  $m$  are the Bohr magneton, Lande factor, magnetic quantum number and mass of atom, respectively. Equations (5) and (8) show that increasing  $B_{1y}$  reduces  $z_{\min}$  and increases frequencies of the traps, respectively. The frequencies of traps are independent of magnetization of the magnetic film. They depend on the external magnetic fields and the periodicity of magnetic lattice.

## 2.2 2D permanent magnetic lattice of microtraps

In order to produce Ioffe-Pritchard microtraps, two crossed layers of periodic arrays of sawtooth magnetic films with two different thicknesses of  $t_1$  and  $t_2$ , separation of  $d$  and same magnetization  $M_z$  with uniform bias fields is investigated (Fig.2). The top and bottom arrays have same periodicity  $a$  along  $x$ - and  $y$ -directions. Thickness of bottom array,  $t_1$  is larger than thickness of top array,  $t_2$ .  $M_z$  is along  $z$ -direction and bias fields are  $B_{1x}$  and  $B_{1y}$ . The

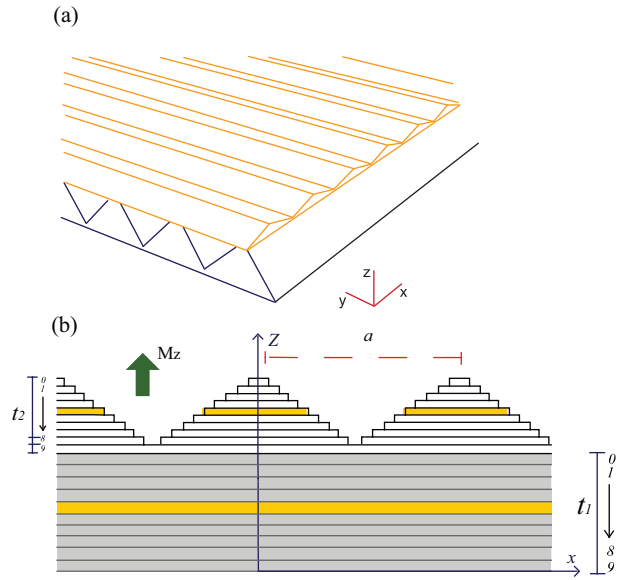


**Fig. 2.** (Color online) (a) Two layers of sawtooth configuration permanent magnetic lattice. (b) Schematic of (a) estimated by  $n=10$  sub-layers of rectangular magnetic slabs for each layer. Top and bottom arrays have corresponding coefficients series  $\lambda_i$  and  $\gamma_i$ , respectively, in magnetic field. Periodicity of top and bottom arrays are  $a=1\mu\text{m}$  along both  $x$ - and  $y$ -directions. Arrays have magnetization  $M_z=3.8$  kG along the  $z$ -direction and thickness  $t_1=500\text{nm}$  and  $t_2=50\text{nm}$  for bottom and top arrays, respectively.

components of the magnetic field, for the large distances ( $k(z-t_1-t_2) \gg 1$ ) from top of the surface can be obtained by

$$B_x = B_{0\lambda} \sin(kx)e^{-kz} + B_{1x} \quad (9)$$

$$B_y = B_{0\gamma} \sin(ky)e^{-kz} + B_{1y}$$

$$B_z = (B_{0\gamma} \cos(ky) + B_{0\lambda} \cos(kx))e^{-kz} + B_{1z}$$

where  $B_{0\lambda} = B_0 \sum \lambda_i$ . Coefficient of the  $i$ th sublayer of infinite magnets of the top array,  $\lambda_i$  is determined, similarly

$$\lambda_i = \frac{1}{A} \sum_{j=0}^i \cos \left( \frac{(2j+1)ka}{4n} \right) (e^{k \frac{t_2}{n}} - 1) e^{k((1-\frac{(i+1)}{n})t_2 + t_1 + d)} \quad (10)$$

where  $d$  is the gap between bottom and top arrays. The magnitude of magnetic field above the surface can be written

$$B(x, y, z) = (B_{1x}^2 + B_{1y}^2 + B_{1z}^2 + 2[B_{0\lambda}B_{1x} \sin(kx) + B_{0\gamma}B_{1y} \sin(ky) + B_{0\lambda}B_{1z} \cos(kx) + B_{0\gamma}B_{1z} \cos(ky)]e^{-kz} + [B_{0\lambda}^2 + B_{0\gamma}^2 + 2B_{0\lambda}B_{0\gamma} \cos(kx) \cos(ky)])^{1/2} \quad (11)$$

Non-zero minimum of the magnetic field and the center of microtraps in  $x$ -,  $y$ - and  $z$ -directions for  $B_{1z}=0$  can be determined by

$$B_{\min} = \frac{|B_{1x}B_{0\lambda} - B_{1y}B_{0\gamma}|}{(B_{0\gamma}^2 + B_{0\lambda}^2)^{1/2}} \quad (12)$$

$$x_{\min} = (n_x + \frac{1}{4})a \quad (13)$$

$$y_{\min} = (n_y + \frac{1}{4})a$$

$$z_{\min} = \frac{1}{k} \ln \left( \frac{\alpha B_{0\lambda}}{B_{1x}} \right)$$

where  $n_x$  and  $n_y$  are number of microtraps and take 0,  $\pm 1, \pm 2, \dots$  values. Dimensionless constant  $\alpha$  is  $(1/2)(1+1/\alpha_0^2)$  where  $\alpha_0 = B_{0\lambda}/B_{0\gamma}$ . At the center of 3D microtraps, the curvature of magnetic fields and barrier heights can be obtained by

$$\frac{\partial^2 B}{\partial x^2} = \frac{\partial^2 B}{\partial y^2} = \frac{1}{2} \frac{\partial^2 B}{\partial z^2} = k^2 \alpha_1 |B_{1x}| \quad (14)$$

$$\Delta B^x = \Delta B^y = \alpha_2 |B_{1x}| \quad (15)$$

$$\Delta B^z = (1 + \alpha_0^2)^{1/2} |B_{1x}|$$

where  $\alpha_1$  and  $\alpha_2$  are

$$\alpha_1 = \frac{2\alpha_0^2}{(1 + \alpha_0^2)^{1/2} |1 - \alpha_0|} \quad (16)$$

$$\alpha_2 = (1 + \alpha_0^2 + \frac{4\alpha_0^2}{1 + \alpha_0^2})^{1/2} - \frac{|1 - \alpha_0^2|}{(1 + \alpha_0^2)^{1/2}}$$

The frequencies of microtraps in three directions are

$$\omega_x = \omega_y = \frac{\omega_z}{\sqrt{2}} = k \left( \frac{\mu_B g_F m_F B_{1x} \alpha_1}{m} \right)^{1/2} \quad (17)$$

For a symmetrical 2D magnetic lattice, same magnetic height barriers in  $x$ - and  $y$ -directions,  $\Delta B^x = \Delta B^y$  are needed. The constraint of  $B_{1y} = \alpha_0 B_{1x}$  satisfies our request where  $\alpha_0 = B_{0\lambda}/B_{0\gamma}$ .

### 2.3 Corresponding magnetic coefficients of estimated layers

The components of magnetic field for  $n_r$  infinitely long and thin permanent magnetic slabs along the  $x$ -direction arranged with periodicity  $a$  along the  $y$ -direction and separation distance  $a/2$  between the center of neighboring slabs, are given by [29]

$$(18)$$

$$B_x = 0$$

$$B_y = B_{0y} \sin(ky) e^{-kz}$$

$$B_z = B_{0y} \cos(ky) e^{-kz}$$

where  $k$  and  $B_{0y}$  are  $2\pi/a$  and  $B_0(e^{kt}-1)$ , respectively. As we mentioned earlier in 2.1 and 2.2, permanent magnetic slabs with sawtooth geometry can be estimated by  $n$

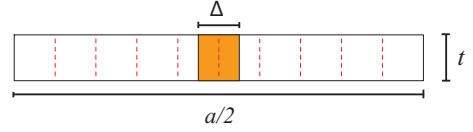


**Fig. 3.** (Color online) Schematic of one slab in permanent magnetic array with periodicity  $a$  and width  $a/2$ . Slabs divided into arbitrary (e.g.  $n=10$ ) narrow slabs  $\Delta$  with same periodicity. The magnetic field of narrow slabs related to initial one by coefficient  $c_1$ . In Eq.19 to obtain  $c_1$ , slab  $\Delta$  shifted to right and left sides by small steps  $\Delta(i+1/2)$ , where  $i=0, 1, \dots, n/2-1$ . Summations are taken on all dashed spaces and results are compared with magnetic field of large slab to find  $c_1$ .

multi-layer arrays of rectangular magnets with same periodicity  $a$  and different width  $w_i$ , where  $i$  is the number of a specific sublayer. The major problem is the calculation of magnetic field of sub-layers with  $w_i > a/2$  or  $w_i < a/2$ . In other words, for magnetic slabs with different width and separation, Eq.18 does not work and needs to be modified. As Fig.1 (b) shows, width plus separation between neighboring slabs for each sublayer  $i$  is constant and equal to periodicity of the lattice. It means that for any modification of Eq.18,  $k$  remains unchanged. The new components of magnetic field for slabs with arbitrary width are related to Eq.18 by coefficient  $\gamma$ . The slabs of periodic lattice by width and separated gap  $a/2$  can be divided into  $n$  narrow slabs (Fig.3) with width  $\Delta=a/2n$ . The magnitude of magnetic field due to these narrow slabs is related to the initial slab with coefficient  $c_1$ . For the calculating of  $c_1$ , narrow slabs can be shifted by small steps of  $a/4n$  along  $y$  axis to make initial array. The component of the magnetic field for these shifted narrow slabs, for example in  $y$ -direction must be consistent with Eq.18, so we have

$$B_{\Delta,y} = c_1 B_{0y} \sum_{j=0}^{n/2-1} \sin k(y \pm (2j+1)\Delta) e^{-kz} \quad (19)$$

$$= B_{0y} \sin(ky) e^{-kz}$$

where  $c_1$  is determined

$$c_1 = (2 \sum_{j=0}^{n/2-1} \cos k(y + (2j+1)k\Delta))^{-1} \quad (20)$$

We use these narrow slabs  $\Delta$  as unit to design any periodic lattice by arbitrary slab width  $w_i$  and periodicity  $a$ . In general, the  $\Delta$  slabs must be several times shifted to the right and left to model the given periodic array. These shifts lead to another series in calculation of the magnetic field which is given by

$$\gamma_i = \frac{2}{c_1} \sum_{j=0}^i \cos(2j+1)k\Delta(e^{k\frac{t}{n}} - 1) e^{kt(1-\frac{i+1}{n})} \quad (21)$$

For sawtooth array, all estimated sub-layers have same thickness  $t/n$  and distance from origin  $s_i = 1-(i+1)/n$ .

Summation on  $\gamma_i$  and  $\lambda_i$  for  $n=10$  sub-layers are determined 13.97 and 5.47, while for  $n=20$  sub-layers reduce to 13.02 and 5.45 values, respectively.

### 3 Numerical calculations for magnetic lattice

Numerical calculations for finite arrays of sawtooth magnetic films with finite length were made. Radia Package [30], interfaced to Mathematica software was used to numerically obtain magnetic field for different configurations of magnets in 1D array of waveguides and 2D arrays of 3D microtraps.

#### 3.1 Atom waveguide

Numerical calculations of 1D array of waveguides above the sawtooth surface of the atom chip were performed when bias magnetic field along the  $y$ -direction,  $B_{1y}$  was applied. Thickness  $t = 500\text{nm}$ , periodicity  $a = 1\mu\text{m}$ , magnetization  $4\pi M_z = 3.8\text{kG}$ , finite toothy magnets number  $n_r = 5001$  which is approximated by  $n = 10$  rectangular slabs. In Fig.4, the components of magnetic field of atom chip above the surface are shown where  $B_{1y} = -5\text{G}$ . This configuration may be used as spatial grating to diffract slowly moving atoms. By including  $B_{1x} = -3\text{G}$  parallel to the waveguide axis, center of waveguides becomes non-zero with  $B_{min} = |B_{1x}| = 3\text{G}$  to avoid spin flips of cold atoms. Center of waveguides is at  $z_{min} = 1.29\mu\text{m}$  from bottom of the layer. Magnetic barrier heights along  $y$ - and  $z$ -directions are 7.4 and 2.8G, respectively. The trap frequencies of 2D microtrap in  $y$ - and  $z$ -directions are numerically determined  $2\pi \times 36.7\text{ kHz}$  for  $^{87}\text{Rb}$  atoms. Fig.4 (a) and (b) show excellent agreement with numerical calculations and analytical expressions of magnetic field along  $y$ - and  $z$ -directions for  $z - t \gg a/2\pi$ . Numerically calculated parameters and related analytical expressions for a sawtooth magnetic film with bias fields are listed in table 1. Large curvatures of the magnetic field ( $\sim 10^{10}\text{ G/cm}^2$ ) can be realized in the permanent magnetic lattices due to their high magnetization which a small size of the microtrap is led to high frequencies for efficient trapping and controlling of ultracold atoms. Rate of spin flips transition for single atom in ground state of harmonic waveguide, when nuclear spin is neglected and total spin is spin of single electron, can be written [23]

$$\Gamma = \frac{\pi\omega}{2} e^{\left(\frac{-U_{min}}{\hbar\omega} - \frac{1}{2}\right)} \quad (22)$$

where  $U_{min}$  and  $\omega$  are potential energy minimum and radial oscillation frequency, respectively. Eq.22 works for  $U_{min} \gg \hbar\omega$ . By using table 1, where  $U_{min}/k_B = 201.5\mu\text{k}$  and  $\hbar\omega/k_B = 1.7\mu\text{k}$ , decay life time of trapped  $^{87}\text{Rb}$  atoms in  $F=2$  and  $m_F=2$  state are so long and there are no majorana losses in the waveguides. Thereby, the introduced waveguides can be used to transfer cold atoms over the surface of single layer atom chip along  $x$ -direction without any significant atom losses from the harmonic trap.

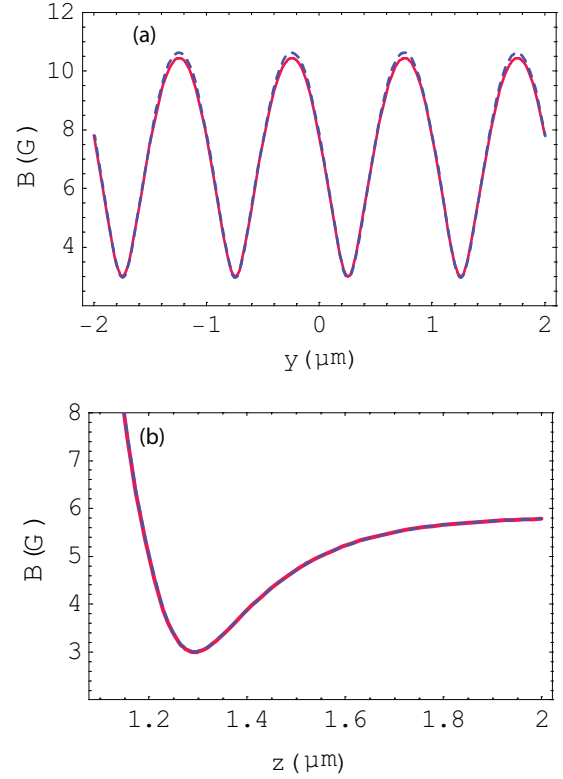


**Fig. 4.** (Color online) (a) and (b) The magnitude of magnetic field close to the center of the waveguides in  $y$ - and  $z$ -directions, respectively. Numerical calculations (red solid) and analytical expressions (dashed-blue) are obtained using Radia and Eq.3, respectively, for  $n=10$  estimated sub-layers. Plots show good versatility between numerical and analytical determinations for  $n_r=5001$  sawtooth slabs with magnetic bias field  $B_{min}=|B_{1x}|=3\text{G}$  and  $B_{1y}=-5\text{G}$ . Center of the waveguides is at  $z_{min}=1.29\mu\text{m}$  and  $y_{min}=(n_y+1/4)a$ , where  $n_y$  is number of waveguides.

#### 3.2 2D permanent magnetic lattice of microtraps

Here, we investigate two crossed sawtooth magnetic layers to create 3D Ioffe-Pritchard microtraps. This magnetic lattice is created when bias fields are applied. Fig.2 shows structure of the atom chip. In each layer, we have considered  $n_r=5001$  parallel long magnets of triangular cross section with magnetization  $4\pi M_z = 3.8\text{kG}$  and periodicity  $a = 1\mu\text{m}$ . The bottom and top layers have thicknesses  $t_1 = 500\text{nm}$  and  $t_2 = 50\text{nm}$ , respectively. The number of sub-layers in each layer is  $n = 10$  and there is no separation between them ( $d = 0$  in Eq.10). Each sawtooth magnetic layer can be estimated by finite number of sublayers of parallel rectangular magnetic slabs with same periodicity, width  $w_i = (i+1)a/n$  and distance  $s_i = (1-(i+1)/n)t$  from the plane  $z = 0$ , where  $i = 0, 1, \dots, n-1$  is the number of the  $i$ th sublayer. To create crossed permanent magnetic sawtooth layers, according to Fig.2(b),  $s_i$  is subject to conditions  $0 < s_i < t_1$  and  $t_1 < s_i < t_2$  for bottom and top arrays, respectively. For  $n=10$  sublayers, great versatility can be seen in Fig.5

**Table 1.** Numerical and analytical determinations for single array of sawtooth permanent magnetic lattice. Lattice has periodicity  $a=1\mu\text{m}$  along  $y$ -direction, thickness  $t=500\text{nm}$  and magnetization  $M_z=3.8\text{ kG}$  along  $z$ -direction (Fig.1(b)). Results is obtained for  $^{87}\text{Rb}$  atoms in different approximation orders (sub-layers) with bias field  $B_{1x}=-3\text{G}$  and  $B_{1y}=-5\text{G}$ .

Parameter	Definition	Numerical		Analytical	
		$n=10$	$n=20$	$n=10$	$n=20$
$n_r$	Number of magnets in $y$ -direction	5001		$\infty$	
$y_{min}(\mu\text{m})$	Center of first waveguide in $y$ -direction	0.25		0.25	
$z_{min}(\mu\text{m})$	Center of waveguides in $z$ -direction	1.29	1.28	1.29	1.28
$\frac{\partial^2 B}{\partial y^2} (\frac{\text{G}}{\text{cm}^2})$	Curvature of B in $y$ -direction	$3.29 \times 10^{10}$		$3.28 \times 10^{10}$	
$\frac{\partial^2 B}{\partial z^2} (\frac{\text{G}}{\text{cm}^2})$	Curvature of B in $z$ -direction	$3.29 \times 10^{10}$		$3.28 \times 10^{10}$	
$\omega_y/2\pi(\text{kHz})$	Trap frequency in $y$ - direction	231.5		231.5	
$\omega_z/2\pi(\text{kHz})$	Trap frequency in $z$ - direction	231.5		231.5	
$B_{min} (\text{G})$	Minimum of B at center of waveguides	3		3	

**Table 2.** Numerical and analytical determinations for two crossed layers of sawtooth permanent magnetic lattice. Lattice has periodicity  $a=1\mu\text{m}$  along  $x$ - and  $y$ -directions, with bottom and top thicknesses  $t_1=500\text{nm}$  and  $t_2=50\text{nm}$  respectively. Two layers have same magnetization  $M_z=3.8\text{ kG}$  along  $z$ -direction (Fig.2(b)). Results are obtained for  $^{87}\text{Rb}$  atoms and bias field  $B_{1x}=-5.6\text{G}$  and  $B_{1y}=-2.18\text{G}$  for  $n=10$  sublayer and  $B_{1x}=-5.6\text{G}$  and  $B_{1y}=-2.3\text{G}$  for  $n=20$  sublayer.

Parameter	Definition	Numerical		Analytical	
		$n=10$	$n=20$	$n=10$	$n=20$
$n_r$	Number of magnets in $x$ - and $y$ -direction	5001		$\infty$	
$x_{min}(\mu\text{m})$	Center of first microtrap in $x$ -direction	0.25		0.25	
$y_{min}(\mu\text{m})$	Center of first microtrap in $y$ -direction	0.25		0.25	
$z_{min}(\mu\text{m})$	Center of microtrap in $z$ -direction	1.33	1.31	1.33	1.31
$\frac{\partial^2 B}{\partial x^2} (\frac{\text{G}}{\text{cm}^2})$	Curvature of B in $x$ -direction	$2.98 \times 10^{10}$		$2.98 \times 10^{10}$	
$\frac{\partial^2 B}{\partial y^2} (\frac{\text{G}}{\text{cm}^2})$	Curvature of B in $y$ -direction	$2.98 \times 10^{10}$		$2.98 \times 10^{10}$	
$\frac{\partial^2 B}{\partial z^2} (\frac{\text{G}}{\text{cm}^2})$	Curvature of B in $z$ -direction	$5.95 \times 10^{10}$	$5.97 \times 10^{10}$	$5.96 \times 10^{10}$	$5.97 \times 10^{10}$
$\omega_x/2\pi(\text{kHz})$	Trap frequency in $x$ - direction	220	220.5	220.3	220.5
$\omega_y/2\pi(\text{kHz})$	Trap frequency in $y$ - direction	220	220.5	220.3	220.5
$\omega_z/2\pi(\text{kHz})$	Trap frequency in $z$ - direction	311.6	312	311.6	312
$B_{min} (\text{G})$	Minimum of B at center of microtraps	4.41	4.27	4.41	4.27

(a), (b) and (c) between analytical and numerical plots of magnetic field along the  $x$ -,  $y$ - and  $z$ -directions, close to the center of the permanent magnetic lattice. By adding more sublayers, we expect to have a sawtooth structure with better accuracy. Numerical and analytical results for the 2D magnetic lattice have been compared in tables 2 and 3 for  $n=10$  and 20, respectively. For example, symmetrical magnetic traps in  $x$ - and  $y$ - directions for  $n=10$  can be obtained at  $z_{min}=1.33\mu\text{m}$  from bottom of the layers by applying the bias field  $B_{1x}=-5.6\text{G}$  and  $B_{1y}=-2.18\text{G}$ . The minimum of the magnetic field at the center of each microtrap is 4.41G.

According to Fig.6, a bias magnetic field along the  $x$ -direction can change the trap frequencies. It is also possible to create permanent magnetic lattices with different barrier heights in the  $x$ - and  $y$ - directions. For example, if we apply a bias magnetic field with  $B_{1x}=-10\text{G}$  and  $B_{1y}=-0.87\text{G}$  the trap depths along the  $x$ - and  $y$ -directions 4.5G and 15G, respectively. For this bias field, correspond-

**Table 3.** Numerical results, using Radia, and analytical ones for  $^{87}\text{Rb}$  in  $F=2$  and  $m_F=2$  state. Results have been calculated for the structure shown in Fig.2.

Parameters ( $\mu\text{k}$ )	Definition	$n=10$	$n=20$
$U_{min}/k_B$	Minimum Potential	296	287
$\Delta U^x/k_B$	Potential barrier height in $x$ -direction	201	213
$\Delta U^y/k_B$	Potential barrier height in $y$ -direction	201	213
$\Delta U^z/k_B$	Potential barrier height in $z$ -direction	107	119
$\hbar\omega_x/k_B$	Energy level spacing in $x$ -direction	10	10
$\hbar\omega_y/k_B$	Energy level spacing in $y$ -direction	10	10
$\hbar\omega_z/k_B$	Energy level spacing in $z$ -direction	15	15

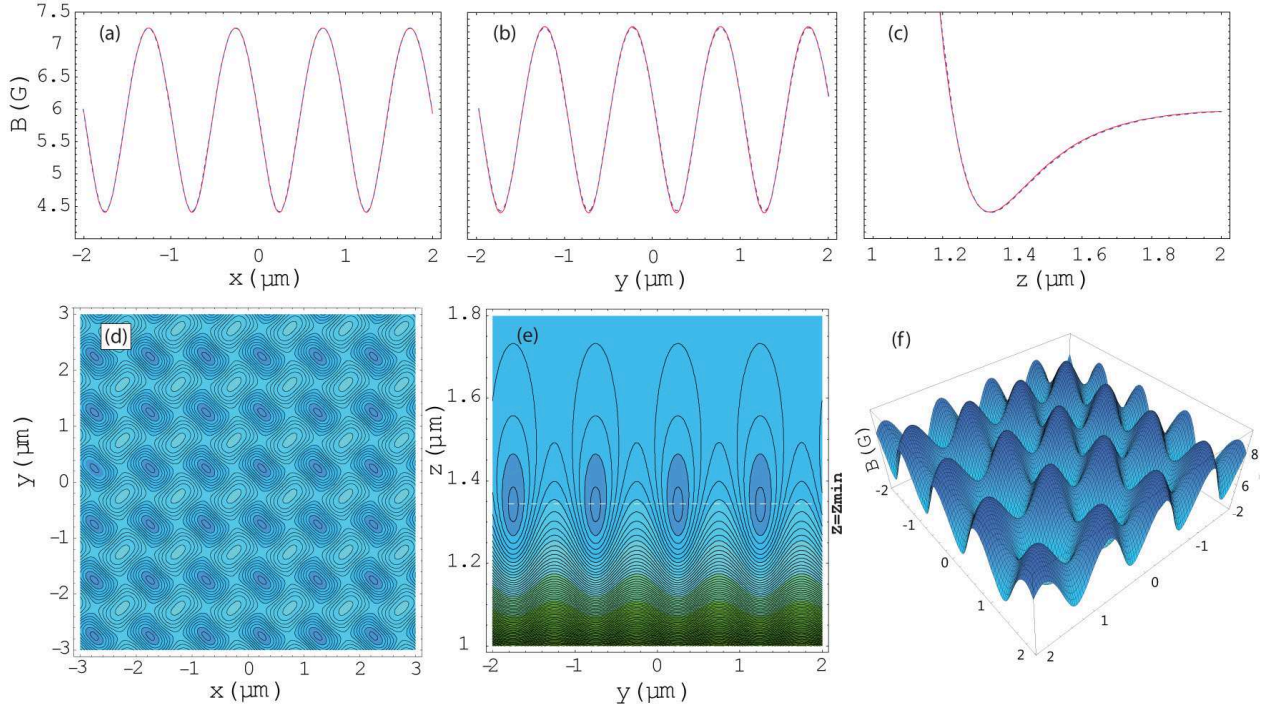


**Fig. 5.** (Color online) (a), (b) and (c) The magnitude of magnetic field close to the center of the microtraps in  $x$ -,  $y$ - and  $z$ -directions, respectively. Numerical calculations (red solid) and analytical expressions (dashed-blue) obtained by Radia and Eq.11 respectively, for  $n=10$  estimated layers. Plots show excellent versatility between numerical and analytical determinations for  $n_r=5001$  sawtooth slabs with magnetic bias field  $B_{1x}=-5.6$  G,  $B_{1y}=-2.18$  G and  $B_{min}=4.41$  G. Center of microtraps along  $z$ -direction is at  $z_{min}=1.33$  μm. Position of first microtrap along  $x$ -and  $y$ -direction is  $x_{min}=y_{min}=0.25$  μm which is repeated by periodicity of arrays. (d) and (e) Contour plots of magnetic field at  $z=z_{min}$  and  $x=x_{min}$  planes, respectively. Yellow points (grey, in black and white) show positions of microtraps. The density of lattice sites is  $\sim 10^6$  traps/mm<sup>2</sup>. (f) 3D plots of magnetic field on the surface of atom chip at  $z=z_{min}$  plane.

ing frequencies along the  $x$ - and  $y$ -directions are not the same and atoms feel two different barrier heights in the  $x$ - and  $y$ -directions, respectively. Decreasing or increasing potential barrier heights will change the rate of tunneling between lattice sites. Different rates is useful in quantum tunnelling experiments.

## 4 Conclusion

We have introduced a new permanent magnetic lattice based on perpendicularly magnetized thin sawtooth films. This lattice can produce Ioffe-Pritchard 2D and 3D microtraps in 1D and 2D lattices, respectively for holding ultracold atoms and BECs when a bias field is applied. We have presented analytical expressions for parameters such as location of the microtraps, curvatures of the magnetic field and also frequencies and trap depth close to the center of the lattice. We also have shown that numerical calculations are in agreement with analytical ones for two different number of the sublayers  $n$ . The components of homogenous external magnetic field along  $x$ - and  $y$ -directions,  $B_{1x}$  and  $B_{1y}$ , can change the trap depth and

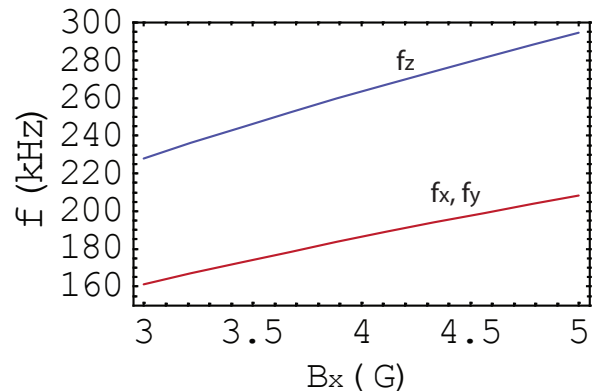


**Fig. 6.** (Color online) Plots show effect of the  $x$  component of the bias field on the trap frequencies for a 2D permanent magnetic lattice.

frequencies of microtraps. Control over the trap depths let us to handle tunneling parameters via increasing or decreasing potential barrier heights for cold atoms and BECs which has wide applications in quantum information processing and superfluid to Mott insulator quantum phase

transition studies. Trap density is  $\sim 10^6$  atoms/mm<sup>2</sup> for loading cold atoms and BECs. Considering the current technology, it should be easy to manufacture the proposed nano-structure.

Amir Mohamadi would like to thank Farhood Ahani and Aref Pariz for helpful discussions.

## References

1. H. J. Metcalf and P. Straten, *Laser Cooling and Trapping*, (Springer, USA, 2002).
2. W. D. Phillips, Rev. Mod. Phys. **70**, 721-741 (1998).
3. M. D. Barrett, J. A. Sauer, and M. S. Chapman, Phys. Rev. Lett. **87**, 010404 (2001).
4. T. Takekoshi, B. M. Patterson, and R. J. Knize, Phys. Rev. Lett. **81**, 5105-5108 (1998).
5. T. W. H. ansch and A. L. Schawlow, Opt. Comm. **13**, 68-69 (1975).
6. J. Mozley *et al.*, Eur. Phys. J. D **35**, 4357 (2005).
7. D. Jaksch, C. Bruder, J. I. Cirac, C. W. Gardiner, and P. Zoller, Phys. Rev. Lett. **81**, 3108-3111 (1998).
8. Y. H. Chen, W. Wu, H. S. Tao, and W. M. Liu, arXiv:1005.0428v2.
9. C. J. Pethick and H. Smith, *Bose-Einstein condensation in dilute gases*, (Cambridge University Press, Cambridge, England, 2008).
10. M. Guglielmino, V. Penna, and B. Capogrosso-Sansone, Phys. Rev. A. **82**, 021601(R) (2010).
11. M. Greiner, O. Mandel, T. Esslinger, T. Hansch, and I. Bloch, Nature, **415**, 39 (2002).
12. J. B. Trebbia, J. Esteve, C. I. Westbrook, and I. Bouchoule, Phys. Rev. Lett. **97**, 250403 (2006).
13. H. van Amerongen, J. J. P. van Es, P. Wicke, K.V. Kheruntsyan, and N. J. van Druten, Phys. Rev. Lett. **100**, 090402 (2008).
14. T. J. Alexander, M. Salerno, E. A. Ostrovskaya, and Yuri S. Kivshar, Phys. Rev. A. **77**, 043607 (2008).
15. M. Nakahara and T. Ohmi, *Quantum computing From Linear Algebra to Physical Realizations*, (CRC Press, USA, 2008).
16. G. Birkl and J. Fortagh, Laser and Photon. Rev. **1**, 12-23 (2007).
17. E. A. Hinds, M. G. Boshier, and I. G. Hughes, Phys. Rev. Lett. **80**, 645-649 (1998).
18. S. Ghanbari, T. D. Kieu, A. Sidorov, and Peter Hannaford, J. Phys. B. **39**, 847-860 (2006).
19. S. Ghanbari, T. D. Kieu, and Peter Hannaford, J. Phys. B: At. Mol. Opt. Phys. **40**, 1283 (2007).
20. D. Muller, D. Z. Anderson, R. J. Grow, P. D. D. Schwindt, and E. A. Cornell, Phys. Rev. Lett. **83**, 1283-1294 (1999).
21. J. Reichel, W. Hnsel, and T. W. Hnsch, Phys. Rev. Lett. **83**, 3398-3401 (1999).
22. C.D.J. Sinclair *et al.*, Eur. Phys. J. D **35**, 105110 (2005).
23. J. Fortagh and C. Zimmermann, Rev. Mod. Phys. **79**, 235 (2007).
24. S. Du and E. Oh, Phys. Rev. A. **79**, 013407 (2009).
25. A. Mohammadi, S. Ghanbari, and A. Pariz, arXiv:1007.2912v1 (2010).
26. T. Fernholz, R. Gerritsma, S. Whitlock, I. Barb, and R. J. C. Spreeuw, Phys. Rev. A. **77**, 033409 (2008).
27. R. Gerritsma *et al.*, Phys. Rev. A. **76**, 033408 (2007).
28. M. Singh, R. McLean, A. Sidorov, and P. Hannaford, Phys. Rev. A. **79**, 053407 (2009).
29. A.I. Sidorov *et al.*, Acta Phys. Pol. B. **33** 2137 (2002).
30. Available from: <http://www.esrf.eu/Accelerators/Groups/InsertionDevices/Software/Radia/Documentation/Introduction>